Kinetic simulations of laser parametric amplification in magnetized plasmas

Qing Jia,[1] Yuan Shi,[1,2] Hong Qin,[1,2,3] and Nathaniel J. Fisch[1,2]
[1]*Department of Astrophysical Sciences, Princeton University, Princeton, New Jersey 08544, USA*
[2]*Princeton Plasma Physics Laboratory, Princeton, New Jersey 08543, USA*
[3]*School of Nuclear Science and Technology, University of Science and Technology of China, Hefei, Anhui 230026, China*

(Received 22 May 2017; accepted 27 July 2017; published online 10 August 2017)

Laser pulse compression using magnetized resonance near the upper-hybrid frequency is promising for achieving higher output intensity in regimes previously thought impossible using unmagnetized plasmas. Using one dimensional particle-in-cell simulations, we verify that, by partially replacing plasma with an external transverse magnetic field of megagauss scale, the output pulse can be intensified by a factor of a few, due to the increased allowable amplification time despite a decreased growth rate. Further improvement is impeded by the generation of an electromagnetic wakefield, to which the amplified pulse loses more energy than it does in the unmagnetized case. This limitation can however be circumvented by the use of a stronger pump. In contrast to unmagnetized compression, the magnetized amplification remains efficient when the pump intensity is well above the wavebreaking threshold, until a higher phase-mixing threshold is exceeded. This surprising resilience to wavebreaking in magnetized plasma is of great benefit for magnetized compression. *Published by AIP Publishing*. [http://dx.doi.org/10.1063/1.4998168]

I. INTRODUCTION

Laser pulses of high intensities and short durations are required in many modern applications, such as inertial confinement fusion and spectroscopic imaging in the nuclear physics beyond the atomic level. Current laser facilities are reaching their intensity limit due to the thermal damage threshold of standard solid-state optical materials. To overcome this limit, parametric amplification in plasma was proposed for next generation laser pulses.[1,2] Intensities up to the exawatt-zetawatt regime are now anticipated.[3]

In the parametric plasma pulse compression scheme, the counter propagating long pump laser and short seed pulse resonantly excite the plasma wave (Langmuir wave for backward Raman amplification (BRA)[1,2] or ion acoustic/quasi-mode wave for Brillouin backward amplification/strongly coupled Brillouin amplification[4–6]) which may grow to large amplitude. The resultant plasma density perturbation acts as a moving Bragg grating, which serves to transfer the energy stored in the long pump to the short seed. Significant theoretical efforts have been exerted to optimize the plasma parametric amplification.[7] Effects of a finite duration, pulse shape, and precursor of the seed pulse were verified.[8–11] Kinetic effects in plasma such as particle trapping,[12] wavebreaking,[13–15] nonlinear Landau damping,[16] and relativistic effects in the saturation regime[17–19] were examined. Multi-dimensional effects such as sidescattering instability[20] and filamentation instability[21–23] were also discussed analytically and numerically. Various methods were proposed for suppressing the premature scattering, such as pulse detuning through pump chirping or plasma density gradient,[24–26] multi-frequency pump,[27] inverse bremsstrahlung stabilization,[28] and amplification in ionizing plasmas.[29–31]

Experimental demonstrations of the plasma parametric amplification were reported.[32–41] Although signatures suggested that the nonlinear regime of the amplification was achieved, the resulting energy transfer efficiency is much lower than that predicted by theory and simulations. One possible explanation for the low efficiency in the BRA is that the density and temperature were not sufficiently uniform for resonant coupling between the pump and the seed.[42] In order to relax this experimental challenge, the parametric amplification in magnetized plasma was recently proposed,[43] where the upper hybrid wave is used instead of the Langmuir wave for the resonance. The contribution from plasma is thus partially replaced by the contribution from the external perpendicular magnetic field, which is easier to control in practice. Besides the improved engineering flexibility, the adverse effects of damping and instabilities are reduced in this kind of magnetized backward Raman amplification (MBRA). It is also possible to extend the intensity and frequency limit of laser pulse compression.

Note that the predictions made in Ref. 43 entailed many simplifications. Foremost, the model is based on the cold fluid approximation. Specifically, for the upper hybrid approximation, the zero temperature asymptote of the electron Bernstein wave (EBW) is generally used. Meanwhile, the electrostatic (ES) approximation for the EBW is applied, where the transverse electric field is assumed to be much smaller than the longitudinal field. In addition, kinetic effects, such as wavebreaking and collisionless damping, were only estimated in the worst case scenario, and the effect of wakefield generation was neglected.

In principle, all these issues can be addressed in particle-in-cell (PIC) simulations. In this paper, we use the PIC code EPOCH[44] in one dimension to model the three wave coupling in magnetized plasma, checking the viability of the MBRA, and quantifying the related scaling laws in Ref. 43. The simulation result supports the general picture of MBRA. However, it also shows that the wakefield generation by the amplified pulse is non-negligible in highly magnetized

plasma, where more energy is lost to the extraordinary electromagnetic wakefield, than that to the electrostatic wakefield excited in unmagnetized or weakly magnetized plasma. In addition, it is found that the previously anticipated limitation due to wavebreaking is bypassed in magnetized amplification. The amplification efficiency remains high even when the pump amplitude is beyond the analytical wavebreaking threshold, until a larger phase-mixing threshold is exceeded. Thus, while verifying the key idea of the MBRA approach, certain refinements on the theory are suggested.

The paper is organized as follows. In Sec. II, we introduce the model describing the 3-wave coupling in MBRA. The setup of the PIC simulations is given in Sec. III, where magnetic field parameters are carefully chosen to excite the appropriate EBW frequency in resonance with the pump and seed. The simulation results, shown in Sec. IV, quantitatively verify the inverse scaling between the linear growth rate and the magnetization factor. The deviations from the analytical prediction in the nonlinear regime are explained by the non-negligible energy loss to the wakefield generation. The resilience to kinetic wavebreaking is investigated at the end of Sec. IV. Summary and conclusions are given in Sec. V.

II. THEORETICAL MODEL

Here, we briefly summarize the basic wave dispersion relationships in the magnetized plasma,[45] as well as the generalized 3-wave interaction model for MBRA. Consider an external magnetic field B_0 in **y** direction, with waves propagating in **x** direction in an isotropic Maxwellian plasma without average flows. The electric field equation can be written as:

$$\begin{pmatrix} \epsilon_{xx} & 0 & \epsilon_{xz} \\ 0 & \epsilon_{yy} - \dfrac{k^2c^2}{\omega^2} & 0 \\ \epsilon_{zx} & 0 & \epsilon_{zz} - \dfrac{k^2c^2}{\omega^2} \end{pmatrix} \begin{pmatrix} E_x \\ E_y \\ E_z \end{pmatrix} = 0, \tag{1}$$

where the components of the dielectric tensor are

$$\epsilon_{xx} = 1 - \frac{\omega_{pe}^2}{\omega}\frac{e^{-\lambda}}{\lambda}\sum_{n=-\infty}^{\infty}\frac{n^2 I_n(\lambda)}{\omega - n\Omega},$$

$$\epsilon_{xz} = -\epsilon_{zx} = i\frac{\omega_{pe}^2}{\omega}e^{-\lambda}\sum_{n=-\infty}^{\infty}\frac{n\left[I_n'(\lambda) - I_n(\lambda)\right]}{\omega - n\Omega},$$

$$\epsilon_{yy} = 1 - \frac{\omega_{pe}^2}{\omega}e^{-\lambda}\sum_{n=-\infty}^{\infty}\frac{I_n(\lambda)}{\omega - n\Omega},$$

$$\epsilon_{zz} = 1 - \frac{\omega_{pe}^2}{\omega}\frac{e^{-\lambda}}{\lambda}\sum_{n=-\infty}^{\infty}\frac{\left[n^2 I_n(\lambda) + 2\lambda^2 I_n(\lambda) - 2\lambda^2 I_n'(\lambda)\right]}{\omega - n\Omega}.$$

Here, $\lambda = k^2\rho_e^2/2$, where $\rho_e = v_{te}/\Omega$ is the electron Larmor radius, $\Omega = eB_0/m_e$ is the electron cyclotron frequency, and ω_{pe} is the plasma frequency. The field equation, Eq. (1), leads to two orthogonal modes. The ordinary (O) wave, whose electric field is *parallel* to $\mathbf{B}_0$, corresponds to $\epsilon_{yy} - k^2c^2/\omega^2 = 0$. The other one, the extraordinary (X) wave, polarized in the plane *perpendicular* to $\mathbf{B}_0$, satisfies

$$\det\begin{pmatrix} \epsilon_{xx} & \epsilon_{xz} \\ \epsilon_{zx} & \epsilon_{zz} - k^2c^2/\omega^2 \end{pmatrix} = 0.$$

For the pump and the seed lasers to couple, they need to have the same polarization, either both be the X mode, or both be the O mode. Since the laser frequency is much larger than the plasma frequency, the cold fluid approximation works well for the pump and the seed. The dispersion relationships for O and X waves in cold fluid approximation are $c^2k^2/\omega^2 = 1 - \omega_{pe}^2/\omega^2$ and $c^2k^2/\omega^2 = RL/S$, respectively. Here, $\begin{smallmatrix}R\\L\end{smallmatrix} = 1 - \omega_{pe}^2/[\omega(\omega \pm \Omega)]$, and $S = (R+L)/2$. The resonantly excited EBW satisfies the same dispersion relationship as the X-wave with non-negligible small thermal correction. When its phase velocity is much less than the speed of light (i.e., $c^2k^2/\omega^2 \gg 1$), the dispersion relationship for EBW can be estimated in the electrostatic approximation as

$$\epsilon_{xx} = 0, \tag{2}$$

which is applicable near upper-hybrid resonance ($\omega \to \omega_{UH} = \sqrt{\omega_{pe}^2 + \Omega^2}$ in the limit $T_e \to 0$).

The general 3-wave coupling process for the MBRA under the ES approximation can be described adequately in terms of a set of equations for the wave envelopes of the laser pulses and EBW[43]

$$(\partial_t + c_a\partial_x)a = \frac{\omega_{pe}}{2}bf, \tag{3}$$

$$\left(\partial_t - c_b\partial_x - i\frac{\omega_{pe}^2}{8\omega_0}b^2\right)b = -\frac{\omega_{pe}}{2}af^*, \tag{4}$$

$$\partial_t f = -\frac{\omega_0\omega_{pe}}{2\omega_3}ab^*. \tag{5}$$

Here, subscript indices denote the respective derivatives; a and b are the amplitudes of the pump and seed pulse, respectively, normalized by $a(b) = eE_{a(b)}/m_e c\omega_{a(b)}$, f is the normalized amplitude of the EBW, $f = eE_f/m_e c\omega_{pe}$. c_a and c_b are the group velocities for the pump and seed, respectively. The resonance frequency ω_3 is the frequency of excited EBW, which is larger than the plasma frequency. The third term in the bracket in the seed pulse equation, Eq. (4), corresponds to the relativistic electron nonlinearity.

From a mathematical point of view, the 3-wave models for MBRA and BRA are the same except for the coupling coefficient. The growth rate in the linear region for MBRA can be similarly obtained as

$$\Gamma_R = \frac{\sqrt{\omega_3\omega_0}}{2}|a_0|/\gamma_B. \tag{6}$$

Here, $\gamma_B = \omega_3/\omega_{pe}$ is the magnetization factor, a_0 is the initial normalized pump amplitude. The amplification process in the nonlinear regime is also predicted to be the same as that in BRA.

In MBRA, although the linear amplification rate is smaller for given resonance frequency due to the lower plasma density, the wave damping and other parametric instabilities that limit the amplification time are even smaller

due to the reduced dependence on internal plasma parameters. This occurs because, while density and temperature fluctuations receive positive feedback through instabilities, the strong external magnetic field does not. Thus, slower amplification within a longer plasma can produce an output pulse with higher intensity in MBRA compared to BRA. In the following, a series of PIC simulations were performed to carefully verify this prediction.

III. SIMULATION SETUP

The main idea of magnetized Raman amplification is to use the magnetic field to make up for the lower density plasma, so as to reduce the damping and parametric instabilities that limit the amplification. Here, we performed PIC simulations to quantify the influence of magnetic field on amplification properties. The scaling laws of the growth rate, amplification time, and saturation intensity as functions of the magnetization factor γ_B for fixed resonance frequency were checked.

Note that in PIC simulations, where the small thermal correction is captured, the frequency of EBW deviates from the upper hybrid resonant frequency. Thus, the choice of external magnetic field strength needs to be made very carefully for the verification of the aforementioned predictions given by a cold fluid model. In practice, we choose the external magnetic field strength based on numerically solving the EBW dispersion relationship in the ES approximation, Eq. (2), which proved to be always valid in the linear regime in our simulation. The example shown in the Appendix illustrates the reduced growth rate and possible envelope modulation of the amplified pulse when the magnetic field is not chosen properly to excite only one branch of the EBW.

For proof-of-principle verification, we use the optical 1 μm wavelength laser as the pump so that collisional and collisionless damping effects are negligible. The linear polarized pump propagates in the negative **x** direction with a temporally constant intensity profile. The temporal Gaussian short seed pulse with a central frequency of 0.905 ω_0 (ω_0 is the pump frequency) and the same polarization as the pump propagates in the positive **x** direction. Electron temperature is initialized as 40 eV in accordance with the estimations in experiments.[35] Ions are kept immobile. The external magnetic field is directed in the **y** direction. The electric fields of both lasers are either in the **y** direction, parallel to the $\mathbf{B}_0$ wherein both lasers become the O-wave; or in the **z** direction, perpendicular to the $\mathbf{B}_0$ and both lasers become the X-wave. Grouped parameters of plasma density and external magnetic field amplitude for simulations with different magnetization factor γ_B are listed in Table. I.

In order to check the saturation regime, we employ a moving-window in our simulations. Any premature scattering of the pump is then not captured. The resolution for all simulations is 100 electrons per cell, 80 cells per laser wavelength, and 85 time steps per laser period, which shows credible converged results when resolution is doubled.

IV. SIMULATION RESULTS ANALYSIS

Our simulation results show that there is little difference for the amplification of O waves and X waves, as long as both the pump and the seed have the same polarization. This is in line with the analytical prediction that the amplification process is independent of the polarization of the laser pulse when laser frequency is much larger than the resonance frequency, as long as the laser propagation direction is perpendicular to the magnetic field. Hereafter, all the discussions will be based on the O-wave for the pump and seed, i.e., the electric fields of both lasers are in **y** direction, parallel to the $\mathbf{B}_0$.

TABLE I. Summary of the grouped parameters of plasma intensity and external magnetic field amplitude for different magnetization factors. Plasma density is normalized to the critical plasma density (n_c) for a 1um pump; external magnetic field amplitude is adjusted in accordance with the plasma density such that the resonance frequency is $\omega_3 = 0.095\ \omega_0$ (thermal effect is considered). The normalization unit $\bar{\mathcal{B}}$ corresponds to the upper hybrid frequency $\sqrt{\omega_{pe}^2 + \left(\frac{e\bar{\mathcal{B}}}{m_e}\right)^2} = 0.095\omega_0$. The magnetic fields are chosen to satisfy $\Omega < \omega_{UH} = \sqrt{\omega_{pe}^2 + \left(\frac{eB_0}{m_e}\right)^2} < 2\Omega$, except in the run.ii where $\omega_{UH} > 3\Omega$.

Run	i	ii	iii	iv	v	vi	vii	viii
$10^3 n_e/n_c$	8.1	7.2	6.3	5.4	4.5	3.6	2.7	1.8
$B_0/\bar{\mathcal{B}}$	NA	0.87	1.432	1.252	1.167	1.122	1.095	1.077
B_0/T	0	278	646	692	745	800	856	909
γ_B	1	1.12	1.20	1.29	1.42	1.58	1.83	2.24

A. Principle verification

The overall temporal evolution of the peak intensities of the amplified pulses is shown in Fig. 1, for cases with different magnetization factors as listed in Table. I. It is observed that, with the increase of γ_B, i.e., with more plasma replaced by the magnetic field, the growth of the amplified pulse becomes slower, but the achievable output pulse intensity is increased by a factor of a few within a longer amplification

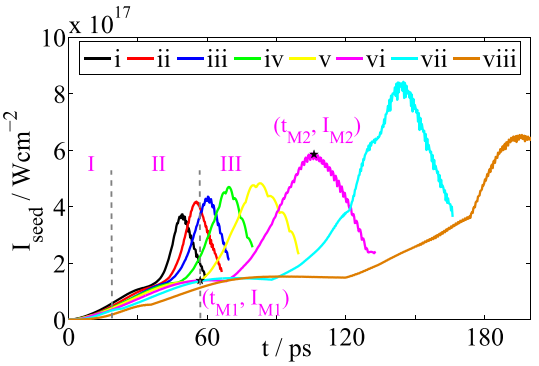

FIG. 1. Temporal evolution of the amplified seed peak intensity for the simulation cases with different magnetization factor γ_B. In all these cases, the pump intensity is 1.37×10^{14} W cm^{-2}, and the initial seed intensity is 2.47×10^{14} W cm^{-2} with a FWHM duration of 150 fs. Other parameters of plasma density and external magnetic field amplitude are listed in Table.1. The overall pulse compression comprises three regimes. Take run.vi as an example, $0 < t < 18$ ps is the first linear amplification regime; $18 < t < 57$ ps is the second nonlinear amplification regime; $t > 57$ ps is the third relativistic nonlinear regime. The stars on the curve mark the weakly relativistic saturation intensity and the final attainable maximum intensity in the strongly relativistic regime for the run.vi.

time. This qualitatively agrees with the theoretical prediction.

The pulse compression demonstrated in the simulations comprises three regimes. First is the linear amplification regime, during which the maximum amplitude of the probed pulse exponentially increases. The qualitative feature is similar to the linear growths shown in Fig. 2(a) where a short weaker seed and stronger pump are used for quantitative comparison with the ideally analytical theory. The growth rates calculated from the slopes shown in Fig. 2(a) are compared with the analytical prediction by the cold fluid model, Eq. (6), as shown in Fig. 2(b). Despite the general lower growth rates in PIC simulations which might be due to the finite duration of seed and thermal corrections, the inverse scaling relationship of the growth rate with the magnetization factor γ_B is in good agreement with the theoretical prediction.

Second is the nonlinear amplification regime when the amplified pulse amplitude is comparable to the pump and the pump depletion is non-negligible. In this regime, the amplified pulse presents the π-pulse-like structure, with the amplitude of its first spike increases linearly with time. Meanwhile, the duration of the first spike of the amplified pulse decreases inversely with time. When the increased pulse intensity approaches 10^{17} W cm^{-2}, the relativistic electron nonlinearity comes into play, and the amplification enters the third relativistic nonlinear regime.

In this third regime, the phase mismatch caused by the relativistic nonlinearity leads to the saturation of the first spike of the amplified pulse, represented by the plateau around 10^{17} W cm^{-2} in each evolution curve shown in Fig. 1. The dependencies of the saturation time and the corresponding saturation intensity on the magnetization factor are plotted in Fig. 3(a). The numerical fitting indicates the

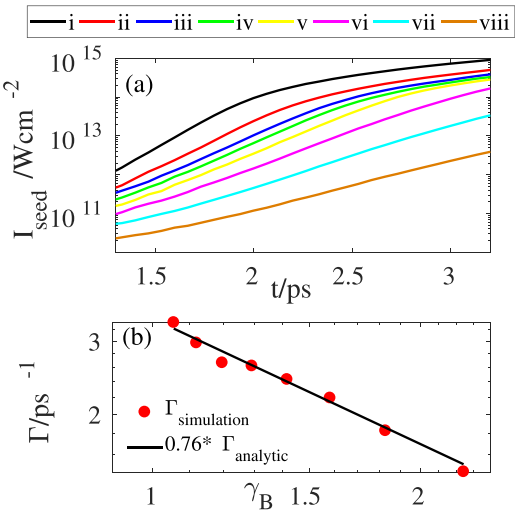

FIG. 2. (a). The temporal evolution of the peak intensity of the probed pulse trailing the seed in the linear amplification regime. (b). The comparison of the linear growth rate obtained from simulations and the analytical prediction. Both axes are in log scale. Here in order to quantitatively compare with the ideally analytical growth rate, an ultrashort seed with low intensity is used and the peak intensity of the trailing probed pulse is tracked. The initial seed intensity in all these cases is 1.37×10^{12} W cm^{-2} with a duration of 30 fs and pump intensity is 3×10^{14} W cm^{-2}. Other parameters are the same as those in Fig. 1.

dependencies as $t_{M1} \sim \gamma_B^{1.5}$ and $I_{M1} \sim \gamma_B^{0.4}$. It roughly agrees with the analytical prediction in Ref. 43: the amplification time limited by the modulational instability scales as $t_M \propto \gamma_B^{4/3}$, and the corresponding peak intensity scales as $I_M \propto \gamma_B^{2/3}$ for cases with the same pump and initial seed. Note that the deviation from the scaling lines becomes large for the last two strongly magnetized cases, which present a smaller peak intensity and a longer amplification time than expected. A possible explanation is the non-negligible seed energy loss resulting from the wakefield generation in the nonlinear amplification regime, as will be investigated in Subsection IV B.

After the saturation of the first spike of the amplified pulse, its second and third spikes reach ever increasing peak intensities shown in Fig. 1. The modulational instability in this highly relativistic regime strongly modulates the pulse envelope, and leads to the final splitting of the pulse, which results in the abrupt decrease of the peak intensity as shown in Fig. 1. The dependence of the attainable maximum intensity and the corresponding amplification time on the magnetization factor is shown in Fig. 3(b). The numerical fitting gives the scaling relationships as $I_{M2} \sim \gamma_B^{0.7}$ and $t_{M2} \sim \gamma_B^{1.7}$. These scalings still roughly agree with the aforementioned predictions, which is based on the consideration of the restriction by modulational instability.

B. Wakefield generation

Careful examination of the electric field during the amplification shows that, besides the laser electric field $\mathbf{E}_y$, the amplitudes of the longitudinal electric field $\mathbf{E}_x$ are always much higher than the transverse electric field $\mathbf{E}_z$ during the initial amplification period, which well supports the ES approximation for EBW. However, with increasing compression of the seed, $\mathbf{E}_z$ increases gradually. While the contribution of $\mathbf{E}_z$ could still be neglected in the weakly magnetized cases, the amplitude of $\mathbf{E}_z$ becomes comparable to $\mathbf{E}_x$ in the last two strongly magnetized cases. As an example, the comparison of the electric fields in run.v ($\gamma_B = 1.42$) and run.viii ($\gamma_B = 2.24$) is shown in Fig. 4.

Note from Fig. 4 that, besides the high frequency oscillations with small amplitudes accounting for the EBW, the $\mathbf{E}_x$ and $\mathbf{E}_z$ fields also present long wavelength modulations, the scale lengths of which are about c/ω_{pe} for each case. These modulations appear to be the wakefields generated by

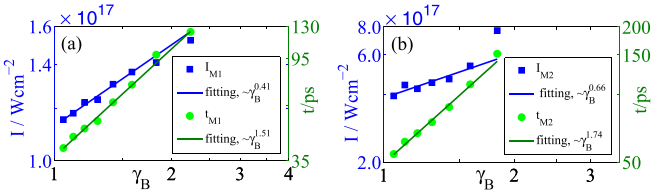

FIG. 3. The relationship of the seed peak intensity (blue squares, left axis) and the amplification time (green dots, right axis) with the magnetization factor γ_B at (a) the weakly relativistic saturation intensity (the moment enters the plateau around 10^{17} W cm^{-2}) and (b) the final attainable maximum intensity in strongly relativistic regime. These data are based on the results shown in Fig. 1. The fitting lines are based on the first six cases, since the results in highly magnetized cases (run.vii and run.viii) obviously deviate from predictions for reasons explained in the text. Both axes are in log scale.

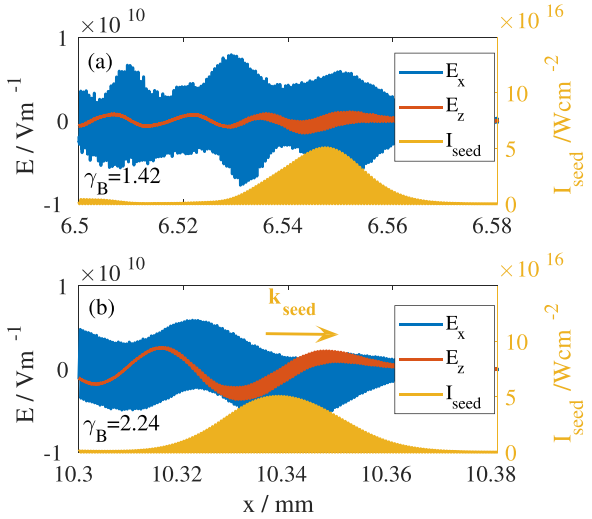

FIG. 4. The snapshots of spatial distributions of the longitudinal electric field ($\mathbf{E}_x$, blue, left axis), transverse electric field ($\mathbf{E}_z$, red, left axis) of the plasma wave and seed intensity (I_{seed}, yellow, right axis) for the case run.v (a) at time $t = 21.8$ ps and run.viii (b) at time $t = 34.3$ ps, when the seed peak intensity increases to 5×10^{16} W cm^{-2} in both cases. The simulation parameters are the same as those shown in Fig. 1. In the weakly magnetized case run.v, transverse $\mathbf{E}_z$ is small compared to longitudinal $\mathbf{E}_x$, in other words, the ES approximation for the EBW is valid for this case. In comparison, the electric fields become comparable in strongly magnetized case run.viii and the ES approximation is not valid.

the propagating seeds, whose amplitudes grow with the amplifying seeds. As noted in Ref. 46, in strongly magnetized plasma ($\Omega/\omega_{pe} \gtrsim 2$), the wakefield excited by the propagating laser pulse is the extraordinary mode with a significant electromagnetic component, rather than the electrostatic upper-hybrid mode in weakly magnetized plasma, and the energy loss rate of the driving pulse increases rapidly in the strongly magnetized case. Thus, the amplification is less efficient due to the larger seed energy loss by the generation of wakefield in the last two cases, which results in the final amplified seed intensity less than the theoretical prediction.[43]

C. Wavebreaking and phase mixing

The pump amplitudes in the last four cases are beyond the wavebreaking threshold[43,47,48]

$$a_{br} = (\omega_3/2\omega_0)^{3/2}/\gamma_B. \tag{7}$$

Thus, one might suspect that the low efficiencies in the last two cases are due to wavebreaking. However, we surprisingly find that the pump depletion rate, often used to indicate the amplification efficiency, remains high for all these simulations.

To find out the origin of this resilience to wavebreaking, we look into the electron dynamics in run.viii and compare to cases with lower and higher pump intensities as shown in Fig. 5. As can be observed, the electron density distributions in the case with pump intensity below the wavebreaking threshold [Fig. 5(d)] and two times above the wavebreaking threshold [Fig. 5(e)] are quite similar. The electron phase plot in the strongly magnetized case [Fig. 5(b)] shows that, due to the restoring force provided by the external magnetic field, the electron sheets do not cross each other, even when the quiver velocity exceeds the phase velocity ($0.05c$). As a result, the EBW can still coherently scatter the pump to amplify the seed effectively. The amplification efficiency in this case is about 66%, much larger than the predicted efficiency in the wavebreaking regime, $(a_{br}/a_0)^2 \simeq 21\%$. In comparison, with an ever larger pump, the quiver velocity becomes too large that the magnetic force is unable to restore the fast electrons. Therefore, phase-mixing happens as shown in Fig. 5(c). The electron density perturbation then becomes anharmonic, where wave energy spreads to higher harmonics, which do not contribute to the pulse compression. Correspondingly, the amplification becomes inefficient with the pump depletion rate of about 11% in the last case. In addition, we checked that the spectra of the amplified seeds differ little for the three cases.

Note that the coherent amplification in the wavebreaking regime of MBRA is different from that found in BRA for an ultrashort pulse.[15] In the case of BRA, the amplification is due to the undepleted Langmuir wave inside the seed region, when the seed duration is shorter than the characteristic wavebreaking time of the Langmuir wave ($\sim\omega_{pe}^{-1}$). The Langmuir wave outside the seed regime is depleted and no longer contributes to the amplification. However, in MBRA, we found that the EBW is resilient to high pump intensity and still survives even when the wavebreaking threshold is exceeded, as long as the magnetic force can restore the electron back to its

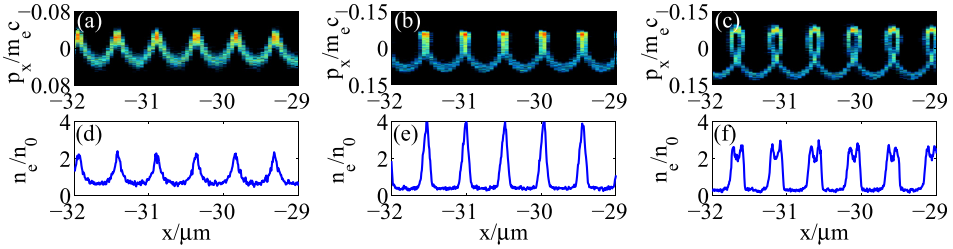

FIG. 5. The snapshots of the electron phase space (b) and the electron density distribution (e) for the run.viii (the normalized pump amplitude is 0.01) shown in Fig. 1. (a) and (d) and (c) and (f) are the corresponding snapshots for the cases with lower pump intensity (the normalized pump amplitude is 0.003) and higher pump intensity (the normalized pump amplitude is 0.03), respectively. Other parameters are the same as those in run.viii. The analytical wavebreaking threshold of the normalized pump amplitude for this parameter setting is $a_{br} = 0.0046$. The snapshots are taken at the time when the seed pulse peak (positioned at $x = 0$ in this figure) intensity is amplified by the same order (from 2.47×10^{14} W cm^{-2} to 5×10^{15} W cm^{-2}) and pump shows distinct depletion. The plasma wave in the first two cases shows a rather coherent structure which effectively scatters pump, while the phase-mixing in the last case leads to the low compression efficiency.

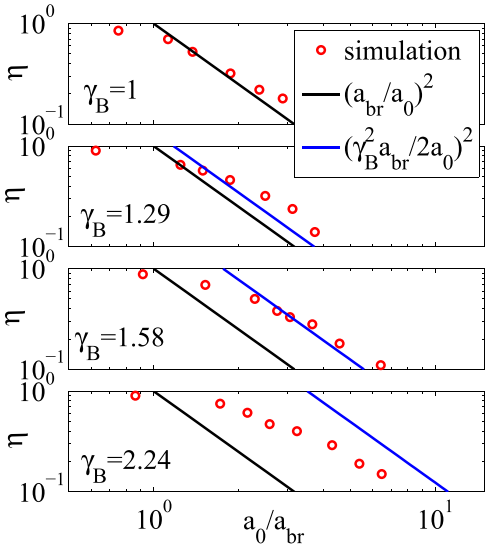

FIG. 6. Efficiency of Raman amplification in the wavebreaking regime. Except for the increasing pump intensities, other parameters are the same as those in run.i, run.iv, run.vi, and run.viii shown in Fig. 1.

original trough. Therefore in MBRA, phase-mixing, instead of wavebreaking, is what imposes the limit on the maximum pump intensity for efficient compression. Above that phase-mixing limit, the EBW loses its coherence and the amplification efficiency falls precipitously.

Here, we heuristically estimate the threshold of phase-mixing in magnetized plasma. As stated above, phase-mixing happens when the Lorentz force can no longer restore the excessive electron quiver velocity in the direction of wave propagation within one wave period

$$e(v_{qt}B_0 - E_f) < m\omega_3(v_{ql} - v_{ph}), \tag{8}$$

where v_{ph} is the phase velocity of the EBW and v_{qt} and v_{ql} are the electron quiver velocity in the direction transverse and longitudinal to the EBW. In the fluid limit, the quiver velocity can be obtained as

$$v_{ql} = \frac{eE_f}{m\omega_{pe}}\frac{\omega_3}{\omega_{pe}}, \quad v_{qt} = \frac{eE_f}{m\omega_{pe}}\frac{\Omega}{\omega_{pe}}. \tag{9}$$

Substituting the above quiver velocities into Eq. (8), we see that phase-mixing happens when $f > \omega_3^2/4\omega_0\omega_{pe}$. Note that this estimation works under the assumption $v_{qt}B_0 > E_f$, i.e., $\gamma_B > \sqrt{2}$, as indicated by Eq. (8). Considering the relationship of $a_0 = \sqrt{\frac{\omega_3}{2\omega_0}}f$ based on energy conservation, where the factor 2 comes from the consideration that the pump slice losing energy within a given plasma layer is twice thicker,[7] the phase-mixing threshold for the pump can be obtained as

$$a_{pm} = \frac{\gamma_B}{2}\left(\frac{\omega_3}{2\omega_0}\right)^{3/2} = \gamma_B^2 a_{br}/2. \tag{10}$$

In order to check this simple estimation, a series of parameter scan simulations are performed and the dependence of the amplification efficiency on the pump intensity is shown in Fig. 6. It can be seen that the depletion rate in unmagnetized plasma ($\gamma_B = 1$) agrees with the analytical prediction as $\eta \approx (a_{br}/a_0)^2$. In the magnetized plasma, the pump depletion rate remains rather high even when the pump amplitude is beyond the wavebreaking threshold. It fails to remain high only when the phase mixing happens. The amplification efficiency agrees well with the estimation $\eta \approx (a_{ph}/a_0)^2$ for the moderately magnetized case ($\gamma_B = 1.58$), while it is higher in the weakly magnetized case ($\gamma_B = 1.29$) and lower in the strongly magnetized case ($\gamma_B = 2.24$) than the above simple estimations. A more accurate derivation of the phase-mixing threshold would require a more comprehensive consideration of the deformed wave structure, which is beyond the scope of this paper.

V. CONCLUSION

The viability of laser pulse compression using magnetic resonance is verified by a series of one dimensional PIC simulations. In the simulations, magnetic field strengths are chosen carefully so that the pump and seed lasers are in resonance via electron Bernstein waves near the upper-hybrid frequency. We verify that such resonance can be excited by lasers of either extraordinary or ordinary mode, and the pulse compression for both polarizations is the same when the laser frequency is much larger than the resonance frequency of the plasma wave. The linear growth rates measured from simulations, which are inversely proportional to the magnetization factors, are in good agreement with the analytical theory. Moreover, the saturation time is demonstrated to increase with increasing magnetization factor due to the reduction of the modulational instability. The net consequence of these two competing effects is an increase of the maximum output pulse intensity by a factor of a few, which is in reasonable agreement with theory.

In addition to verifying the basic analytical theory, our simulations also demonstrate the importance of two kinetic effects. The first is wakefield generation, through which the amplified pulse loses its energy. For a larger magnetization factor, the wakefield contains a larger electromagnetic component, which takes away more energy from the amplified pulse. The second kinetic effect is phase-mixing, through which the plasma wave loses coherence and thereafter no longer mediates pulse compression. Unlike in the unmagnetized cases, our simulation results demonstrate that the magnetized resonance remains coherent even when the pump amplitude is beyond the wavebreaking threshold. Due to this resilience to wavebreaking, a larger intensity pump can be used in magnetized plasma to achieve even higher output intensity than previously thought.

As a proof-of-principle verification, we only consider the amplification of the optical lasers where the collisional and collisionless damping effects are negligible. The verification of the expanded operation window of MBRA,[43] which is particularly appealing for UV-waves and X-rays where the damping effects play an important role, remains to be done through more extensive simulations than those presented here.

ACKNOWLEDGMENTS

This work was supported by the NNSA Grant No. DE274-FG52–08NA28553 and AFOSR Grant No. FA9550–15-

1–0391. The simulations were performed at PPPL's Research Computing Center. The development of the EPOCH code was funded in part by UK EPSRC Grant Nos. EP/G054950/1, EP/G056803/1, EP/G055165/1, and EP/M022463/1.

APPENDIX: PARAMETER CHOOSING

One of the interesting phenomena in MBRA is the possibility of simultaneously exciting two or more EBW modes. In unmagnetized BRA, the Langmuir wave with a corresponding frequency is excited for a fixed wavenumber ($k \simeq 2k_0$, where k_0 is the wavenumber of light in plasma.) However, in MBRA, due to the many branches of the EBW modes, two or more modes with close frequencies can be excited for a fixed wavenumber. Figure 7 compares the seed profiles for two different external magnetic field cases. In the imperfect matching case, the external magnetic field is such that the upper hybrid frequency right equals the difference between the pump and seed, $\sqrt{\omega_{pe}^2 + \left(\frac{e\bar{\mathcal{B}}}{m_e}\right)^2} = \omega_{pump} - \omega_{seed}$. However, due to the thermal corrections, what is actually being excited are the two EBW modes that reside above and below the upper hybrid resonance, which correspond to the resonant seed frequencies of $0.9\omega_0$ and $0.93\omega_0$, respectively. The beating of the two excited modes leads to the envelope modulations in the amplified seed profile shown in Fig. 7(a). The spectral analysis [Fig. 7(c)] shows good agreement with the modes results from the analytical EBW dispersion relationship [Fig. 7(e)]. In comparison, Figs. 7(b), 7(d), and 7(f) show the case with an external magnetic field amplitude of $0.92\bar{\mathcal{B}}$, where the excited EBW mode frequency is right of the difference of pump and seed frequency. The spectral analysis of this case still shows a subdominant spike at frequency $0.94\omega_0$, which corresponds to the EBW mode below the upper hybrid frequency, as shown in Fig. 7(f). However, this mode shows little amplification due to smaller growth rate, which leads to scarce modulations in the amplified seed profile. From the comparison of the two cases, it is noted that the right choice of external magnetic field amplitude is of great importance for efficient amplification.

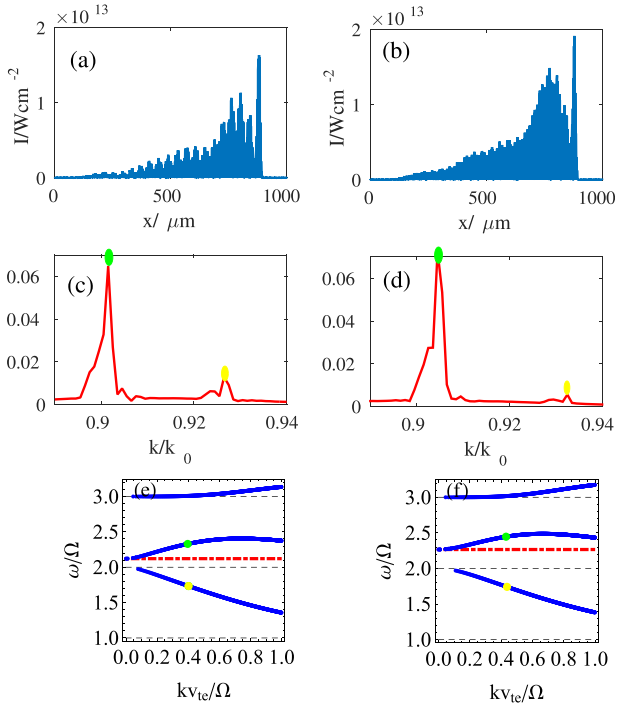

FIG. 7. (a) and (c) and (b) and (d) are snapshots of the amplified seed profile and the corresponding spectra in the mismatch case ($B_0 = \bar{\mathcal{B}}$) and matching case ($B_0 = 0.92\bar{\mathcal{B}}$), respectively. (e) and (f) are the dispersion relationships of the EBW in the ES approximation for the $B_0 = \bar{\mathcal{B}}$ and $B_0 = 0.92\bar{\mathcal{B}}$ cases, respectively. The green and yellow points in (e) and (f) correspond to the peak modes marked in (c) and (d). Note that in (a), (c), and (e), plasma parameters are chosen to match the cold resonance [red dashed line in (e)], but due to the thermal effect, what actually been excited are the two EBW modes (green and yellows points). In comparison, in (b), (d), and (f), plasma parameters are chosen to match one EBW (green point), so that the other EBW (yellow point) is subdominant.

[1]G. Shvets, N. J. Fisch, A. Pukhov, and J. Meyer-ter Vehn, Phys. Rev. Lett. **81**, 4879 (1998).
[2]V. M. Malkin, G. Shvets, and N. J. Fisch, Phys. Rev. Lett. **82**, 4448 (1999).
[3]G. Mourou, N. Fisch, V. Malkin, Z. Toroker, E. Khazanov, A. Sergeev, T. Tajima, and B. L. Garrec, Opt. Commun. **285**, 720 (2012).
[4]A. A. Andreev, C. Riconda, V. T. Tikhonchuk, and S. Weber, Phys. Plasmas **13**, 053110 (2006).
[5]M. R. Edwards, Q. Jia, J. M. Mikhailova, and N. J. Fisch, Phys. Plasmas **23**, 083122 (2016).
[6]M. Chiaramello, F. Amiranoff, C. Riconda, and S. Weber, Phys. Rev. Lett. **117**, 235003 (2016).
[7]V. Malkin and N. Fisch, Eur. Phys. J. Spec. Top. **223**, 1157 (2014).
[8]N. A. Yampolsky, V. M. Malkin, and N. J. Fisch, Phys. Rev. E **69**, 036401 (2004).
[9]G. Lehmann, K. H. Spatschek, and G. Sewell, Phys. Rev. E **87**, 063107 (2013).
[10]Q. Jia, I. Barth, M. R. Edwards, J. M. Mikhailova, and N. J. Fisch, Phys. Plasmas **23**, 053118 (2016).
[11]Y. A. Tsidulko, V. M. Malkin, and N. J. Fisch, Phys. Rev. Lett. **88**, 235004 (2002).
[12]M. S. Hur, R. R. Lindberg, A. E. Charman, J. S. Wurtele, and H. Suk, Phys. Rev. Lett. **95**, 115003 (2005).
[13]Z. Toroker, V. M. Malkin, and N. J. Fisch, Phys. Plasmas **21**, 113110 (2014).
[14]M. R. Edwards, Z. Toroker, J. M. Mikhailova, and N. J. Fisch, Phys. Plasmas **22**, 074501 (2015).
[15]J. P. Farmer and A. Pukhov, Phys. Rev. E **92**, 063109 (2015).
[16]N. A. Yampolsky and N. J. Fisch, Phys. Plasmas **16**, 072105 (2009).
[17]V. M. Malkin, Z. Toroker, and N. J. Fisch, Phys. Plasmas **21**, 093112 (2014).
[18]V. M. Malkin, Z. Toroker, and N. J. Fisch, Phys. Rev. E **90**, 063110 (2014).
[19]I. Barth, Z. Toroker, A. A. Balakin, and N. J. Fisch, Phys. Rev. E **93**, 063210 (2016).
[20]A. A. Solodov, V. M. Malkin, and N. J. Fisch, Phys. Rev. E **69**, 066413 (2004).
[21]R. M. G. M. Trines, F. Fiuza, R. Bingham, R. A. Fonseca, L. O. Silva, R. A. Cairns, and P. A. Norreys, Nat. Phys. **7**, 87 (2011).
[22]G. Lehmann and K. H. Spatschek, Phys. Plasmas **21**, 053101 (2014).
[23]C. Riconda, S. Weber, L. Lancia, J.-R. Marquès, G. Mourou, and J. Fuchs, Plasma Phys. Controlled Fusion **57**, 014002 (2015).
[24]V. M. Malkin, G. Shvets, and N. J. Fisch, Phys. Rev. Lett. **84**, 1208 (2000).
[25]V. M. Malkin, G. Shvets, and N. J. Fisch, Phys. Plasmas **7**, 2232 (2000).
[26]B. Ersfeld and D. A. Jaroszynski, Phys. Rev. Lett. **95**, 165002 (2005).
[27]A. A. Balakin, G. M. Fraiman, N. J. Fisch, and V. M. Malkin, Phys. Plasmas **10**, 4856 (2003).
[28]R. L. Berger, D. S. Clark, A. A. Solodov, E. J. Valeo, and N. J. Fisch, Phys. Plasmas **11**, 1931 (2004).
[29]V. M. Malkin and N. J. Fisch, Phys. Plasmas **8**, 4698 (2001).
[30]D. S. Clark and N. J. Fisch, Phys. Plasmas **9**, 2772 (2002).
[31]D. S. Clark and N. J. Fisch, Phys. Plasmas **10**, 4837 (2003).
[32]Y. Ping, I. Geltner, N. J. Fisch, G. Shvets, and S. Suckewer, Phys. Rev. E **62**, R4532 (2000).

[33]Y. Ping, I. Geltner, A. Morozov, N. J. Fisch, and S. Suckewer, Phys. Rev. E **66**, 046401 (2002).
[34]Y. Ping, W. Cheng, S. Suckewer, D. S. Clark, and N. J. Fisch, Phys. Rev. Lett. **92**, 175007 (2004).
[35]W. Cheng, Y. Avitzour, Y. Ping, S. Suckewer, N. J. Fisch, M. S. Hur, and J. S. Wurtele, Phys. Rev. Lett. **94**, 045003 (2005).
[36]J. Ren, W. Cheng, S. Li, and S. Suckewer, Nat. Phys. **3**, 732 (2007).
[37]R. K. Kirkwood, E. Dewald, C. Niemann, N. Meezan, S. C. Wilks, D. W. Price, O. L. Landen, J. Wurtele, A. E. Charman, R. Lindberg, N. J. Fisch, V. M. Malkin, and E. O. Valeo, Phys. Plasmas **14**, 113109 (2007).
[38]C.-H. Pai, M.-W. Lin, L.-C. Ha, S.-T. Huang, Y.-C. Tsou, H.-H. Chu, J.-Y. Lin, J. Wang, and S.-Y. Chen, Phys. Rev. Lett. **101**, 065005 (2008).
[39]Y. Ping, R. K. Kirkwood, T.-L. Wang, D. S. Clark, S. C. Wilks, N. Meezan, R. L. Berger, J. Wurtele, N. J. Fisch, V. M. Malkin, E. J. Valeo, S. F. Martins, and C. Joshi, Phys. Plasmas **16**, 123113 (2009).
[40]L. Lancia, J.-R. Marquès, M. Nakatsutsumi, C. Riconda, S. Weber, S. Hüller, A. Mančić, P. Antici, V. T. Tikhonchuk, A. Héron, P. Audebert, and J. Fuchs, Phys. Rev. Lett. **104**, 025001 (2010).
[41]L. Lancia, A. Giribono, L. Vassura, M. Chiaramello, C. Riconda, S. Weber, A. Castan, A. Chatelain, A. Frank, T. Gangolf, M. N. Quinn, J. Fuchs, and J.-R. Marquès, Phys. Rev. Lett. **116**, 075001 (2016).
[42]N. A. Yampolsky and N. J. Fisch, Phys. Plasmas **18**, 056711 (2011).
[43]Y. Shi, H. Qin, and N. J. Fisch, Phys. Rev. E **95**, 023211 (2017).
[44]T. D. Arber, K. Bennett, C. S. Brady, A. Lawrence-Douglas, M. G. Ramsay, N. J. Sircombe, P. Gillies, R. G. Evans, H. Schmitz, A. R. Bell, and C. P. Ridgers, Plasma Phys. Controlled Fusion **57**, 113001 (2015).
[45]T. H. Stix, *Waves in Plasmas* (Springer Science & Business Media, 1992).
[46]A. Holkundkar, G. Brodin, and M. Marklund, Phys. Rev. E **84**, 036409 (2011).
[47]R. Davidson and P. Schram, Nucl. Fusion **8**, 183 (1968).
[48]C. Maity, A. Sarkar, P. K. Shukla, and N. Chakrabarti, Phys. Rev. Lett. **110**, 215002 (2013).